ACS APPLIED MATERIALS & INTERFACES

Research Article

www.acsami.org

# Beetle-Inspired Bidirectional, Asymmetric Interlocking Using Geometry-Tunable Nanohairs

Changhyun Pang,[†,§] Sang Moon Kim,[†,§] Yudi Rahmawan,[‡] and Kahp-Yang Suh*[,†,‡]

[†]Division of WCU Multiscale Mechanical Design, [‡]School of Mechanical and Aerospace Engineering, Seoul National University, Seoul 151-742, Korea

Supporting Information

**ABSTRACT:** We present bidirectional, asymmetric interlocking behaviors between tilted micro- and nanohair arrays inspired from the actual wing locking device of beetles. The measured shear adhesion force between two identical tilted microhair arrays (1.5 $\mu$m radius, 30 $\mu$m height) turned out to be higher in the reverse direction than that in the angled direction, suggesting that the directionality of beetle's microtrichia may play a critical role in preventing the elytra from shifting along the middle of insect body. Furthermore, we observed dramatic enhancement of shear adhesion using asymmetric interlocking of various nanohair arrays (tilting angle, $\delta < 40°$). A maximum shear locking force of ~60 N/cm$^2$ was measured for the nanohair arrays of 50 nm radius and 1 $\mu$m height with a hysteresis as high as ~3. A simple theoretical model was developed to describe the measured asymmetric adhesion forces and hysteresis, in good agreement with the experimental data.

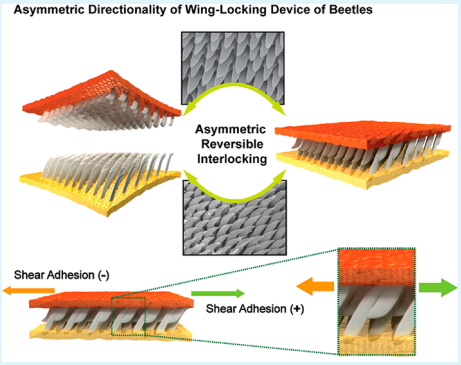


**KEYWORDS:** *biomimetics, interlocking, beetle, nanohairs, dry adhesive*

## INTRODUCTION

Directional, asymmetric surface architecture is an essential feature for many living organisms in nature. Examples include spider-net,[1,2] shell of desert-beetles[3−5] and butterfly wing[6] for directional water transport,[7,8] adherent gecko[9−13] and insect[14−16] for active locomotion, anisotropic wrinkling[17,18] and photonics,[19,20] and shark[21] and snake skins[22] for low frictional surfaces. These unique surface properties have been shedding light on nature-inspired smart materials and devices in a wide range of applications from water/oil repellent surfaces, contamination-free dry adhesives, to directional water harvesting. A number of reviews are available for detailed fabrication methods, mechanisms, and applications.[23−25]

In addition to the above-mentioned examples, one can observe a unique structural device in nature in the form of a reversible mechanical interlocker. A typical example is the interlocking between "hooks" and "loops" in burdock's seeds, which is now commonly used in fabric Velcro. Also, zoologists have observed a unique interlocking structure in insects such as dragonfly's head arrester and beetle's wing.[26,27] Motivated by these observations, we recently reported that a wing-to-body locking device is present in an anterior field of the elytra as well as in an opposite field of thorax, where asymmetric microstructures called $\beta$-keratin microtrichia are reversibly interconnected to fix the wing.[28] In particular, regularly tilted asymmetric corn-shape microhairs are observed in the actual wing locking device, whose functionality in reversible attachment has remained unexplored. This directional, reversible interlocking system is potentially useful for many applications including fastener-type adhesive,[28,29] switchable adhesion,[30,31] electric connector,[32] biomedical patch,[33] and flexible, wet, or thermal responsive adhesive.[29,34,35]

Following our earlier observation on reversible interlocking with vertically oriented hairs,[28,36] we present here bidirectional, asymmetric interlocking between tilted, high aspect-ratio (AR) micro- and nanohairs utilizing geometry-tunable replica molding and broad ion beam irradiation. In the broad ion beam irradiation, the as-formed hairy structures are irradiated by Ar ion beam at a tilting angle (0−90°) with an appropriate intensity and time, thereby changing the bending angle in a precisely controllable manner. This method is advantageous over oblique e-beam irradiation as the structural transformation is completed rapidly (<1 min) on a large area.[37,38] Using this method, we first prepared microscale vertical and tilted hair arrays (tilting angle, $\delta < 40°$) of 1.5 $\mu$m radius, 30 $\mu$m height (SR = 3) with hexagonal layout that appear structurally similar to the beetle's microtrichia. Then, the role of the beetle's bidirectional wing locking device was confirmed. To further exploit asymmetric interlocking behaviors, various stooped nanohair arrays ($\delta < 40°$) were formed and then reversibly interconnected to each other to measure the shear locking force. It turned out that the maximum force was as high as ~60 N/cm$^2$ when the two surfaces having nanohair arrays of 50 nm radius and 1 $\mu$m height were pulled in the reverse direction with respect to the bending angle. The hysteresis in this asymmetric, bidirectional adhesion was measured to be ~3,

Received: May 24, 2012
Accepted: July 20, 2012
Published: July 20, 2012

  

which was in a good agreement with our simple theoretical model.

## EXPERIMENTAL SECTION

**Materials of Various Tilted Nanohairs.** Two polyurethane acrylate (PUA) materials with different rigidity were purchased from Minuta Tech, Korea and used throughout the experiment: PU elastomer for microfiber arrays (elastic modulus: 3 MPa) and soft PUA (MINS 301 RM) for nanofiber arrays (elastic modulus: 19.8 MPa).[39]

**Fabrication of Various Tilted Nanohairs.** At first, vertical micro/nano hair arrays were prepared using hole patterned silicon masters by photolithography and reactive ion etching. The masters were treated with a fluorinated-SAM solution ((tridecafluoro-1,1,2,2-tetrahydrooctyl)-trichlorosilane:FOTCS, Gelest Corp.) diluted to 0.03 M in anhydrous heptane in an Ar chamber. After the surface treatment, the masters were annealed at 120 °C for 20 min. Drops of ~200 $\mu$L of PU elastomer prepolymer (PU elastomer, Minuta Tech, Korea) or soft PUA prepolymer (s-PUA; PUA MINS 301 RM, Minuta Tech, Korea) were dispensed onto the patterned master and a supporting PET film (thickness: 50 $\mu$m) was covered onto the liquid drop, which was slightly pressed to spread the liquid uniformly on the master. Then, the prepolymer was cured under UV light of 100 W/cm$^2$ for ~30 s (Fusion Cure System, Minuta Tech, Korea). The polymer replica was peeled off from the master, leaving behind an array of vertical hairy structures.[39] Next, the as-prepared vertical nanohairs were put into an end-Hall type linear ion gun system (Alcatel Vacuum Technology, France) to irradiate Ar gas to the nanohairs. After evacuating air, the anode voltage was kept constant at 1 keV during ion treatment with a current density of 50 $\mu$A/cm$^2$ and a radio frequency (RF) bias voltage of −600 V was applied to the sample holder with an Ar gas flow rate of 8 sccm for the duration of 1 min. The incident angle of ion beam was varied by tiling the sample holder (40°, 50°, and 65°), resulting in various bending angles of hairs of 15°, 30°, and 40°.[38] For characterization and adhesion tests, six experimental sets were prepared: tilted microhair (0° and 40°) of 1.5 $\mu$m radius and 30 $\mu$m height (PU elastomer) and tilted nanohairs (0°, 15°, 30°, and 40°) of 50 nm radius and 1 $\mu$m height (s-PUA). The spacing ratio (SR) was at 3 for all samples.

**Adhesion Tests.** To analyze asymmetric adhesion properties, the upper and lower surfaces (1 × 1 cm$^2$ area each) of stooped micro- or nanohair arrays were brought into contact with a preload of ~5 N/cm$^2$ and reversibly interconnected. Using custom-built equipment (see Supplementary Figure S1, Supporting Information), a uniform pulling force was applied to the sample with a velocity of 200−3000 $\mu$m/s, until an adhesion failure occurred. A shear velocity of ~200 $\mu$m/s was typically used to hold a substantial weight in consideration of the viscoelastic property (see Supplementary Figure S2, Supporting Information). In this way, shear adhesion forces were measured in the angled (+) and the reverse (−) directions with respect to the initial bending geometry. All measurements were repeated at least 10 times at ambient temperature under a relative humidity of 50%, and average values were used for the plots.

## RESULT AND DISCUSSIONS

Figure 1a shows an illustration of the actual wing locking device of beetle (Promethis valgipes) along with the corresponding SEM images, in which tilted microtrichia on the cuticular surface of hind wing and those on the insect body are interlocked with directionality. The SEM images demonstrate that the microhairs are of a corn shape and angled with pointed directionality. When beetles fold their wings on a tree or a ground, an asymmetric interconnection is expected to occur with bidirectional high shear adhesion as schematized in Figure 1b, while a normal lift-off would be extremely simple and effortless. This wing locking device is highly reversible and does not require additional physical load or surface modification.[28] Figure 1b shows an illustration of directional, asymmetric shear force in the angled (+) and the reverse (−) directions. Here, the (+) direction denotes the direction toward the edge of beetle's torso, while the (−) direction to the center of body. From our close observation, the microtrichia on the beetle's hind-wing (an anterior field of thorax) consist of ~40° tilted microfibers of ~2.2 $\mu$m diameter and ~17 $\mu$m height (AR = ~8) (Figure 1a, right top image). In contrast, the slanted microstructures on the insect body (an anterior field of the elytra) are of ~1.5 $\mu$m diameter and ~15 $\mu$m height (AR = ~10) (Figure 1a, right bottom image) with 40°−50° tilted microfibers. Both structures are regularly ordered with hexagonal packing layout with the spacing ratio (SR) of ~3. Here, SR is defined as the distance between hairs divided by width.

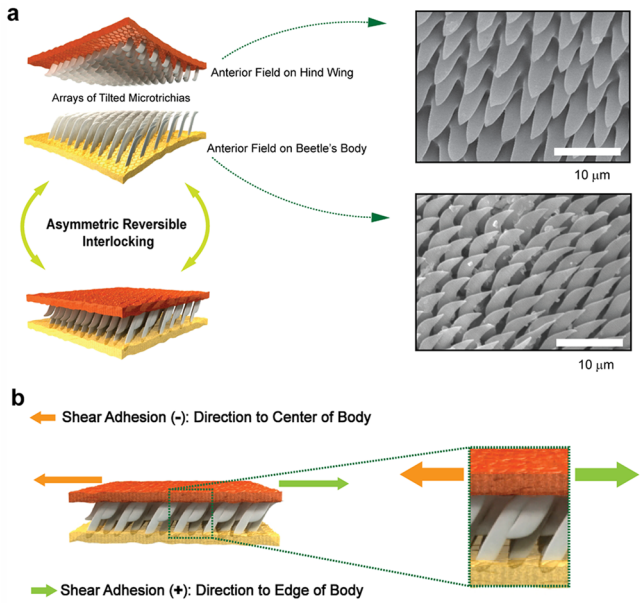


**Figure 1.** (a) Illustration of the actual wing locking device of beetle (*Promethis valgipes*) along with the corresponding SEM images, in which tilted $\beta$-keratin microtrichia on the cuticular surface of hind wing and those on the insect body are interlocked. (b) Illustration of directional, asymmetric shear force in the angled (+) and the reverse (−) directions.

To investigate bidirectional properties of reversible interconnection of the beetle's wing locking device, vertical and tilted microhair arrays ($\delta \sim 40°$) of 1.5 $\mu$m radius and 30 $\mu$m height (SR = 3) were prepared with PU elastomer (elastic modulus: 3 MPa) as shown in Figure 2a,b (see Experimental Section for details and Figure S3, Supporting Information, for large-area images). As can be seen from the images, the

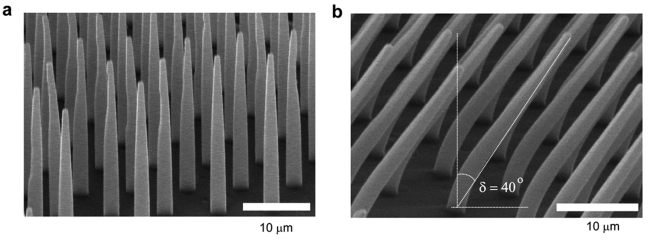


**Figure 2.** (a,b) SEM images of the as-prepared vertical PU elastomer hairs of 1.5 $\mu$m radius and 30 $\mu$m height (SR = 3) with hexagonal layout (a) and the same microfibers after oblique broad ion beam irradiation (b).

microhairs were uniformly fabricated over a large area and nearly straight even in the stooped state. Using these microhairs, the shear adhesion force was measured using custom-built equipment (Supplementary Figure S1, Supporting Information) in the angled (+) and the reverse (−) directions. By applying various preloads from 0.1 N/cm$^2$ to 5 N/cm$^2$, two identical surfaces with vertical or tilted hairs were brought in contact, forming a microstructural interconnection. The measurement of shear adhesion for the three cases is shown in Figure 3. As shown, the shear adhesion forces were increased

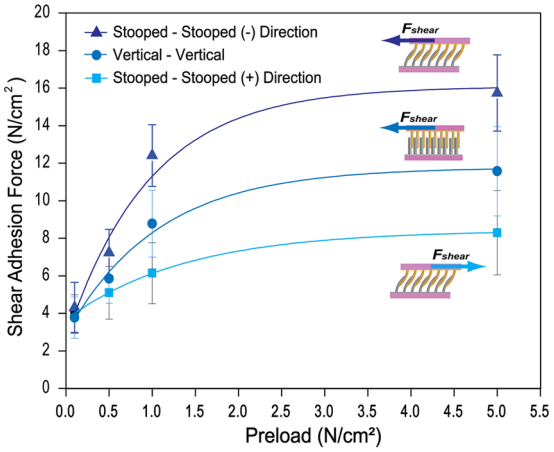


**Figure 3.** Plots of preload dependency of shear adhesion force with 40° stooped−40° stooped and vertical microfiber arrays with preloads in the range of 0.1 to 5 N/cm$^2$.

with the increase of preload from 0.1 N/cm$^2$ to 5 N/cm$^2$ probably due to the elevation of overlapping length between upper and lower hairs.[36] In the case of interlocking between stooped hairs, the measured shear locking forces displayed the maximum of ∼9.5 N/cm$^2$ in the (+) direction and ∼15 N/cm$^2$ in the (−) direction, with the hysteresis being ∼1.6 with the preload of 5 N/cm$^2$. In comparison, the maximal force between two vertical hairs was ∼12.5 N/cm$^2$ under the same preload, which lied between the two values. On the basis of these results, it can be thought that the directionality of microstructures may serve for preventing the elytra from shifting along the middle of insect mass (− direction) so as to fix the delicate wings more safely during folding and unfolding states.

To elaborate on the effect of tilting angle in directional interlocking, we prepared various geometry-controlled nanofiber arrays of 50 nm radius and 1 $\mu$m height (SR = 3) with hexagonal layout and measured shear adhesion using soft PUA material (∼19.8 MPa). Figure 4a−d shows polymeric nanohairs with a range of tilting angles ($\delta \sim 0°$, 15°, 30°, and 40°) via replica molding and oblique broad ion beam irradiation (see Experimental Section for details). The cross-sectional SEM images in Figure 5 provide an insight into how the interlocking contact is mediated by van der Waals force between vertical or tilted ($\delta$ = 40°) nanohairy surfaces. The estimated ratio of overlapping was 60−80% between the upper and lower hairs with some broken and misaligned structures. Also, it is noted that the tilted hairs are preserved during the entire bonding and pulling steps (see yellow box in Figure 5b).

In order to understand the asymmetric interlocking behavior presented here, the step-by-step events that may occur in the course of interlocking and pulling in the (+) and (−) directions are schematically drawn in Figure 6. Also, a simple theoretical

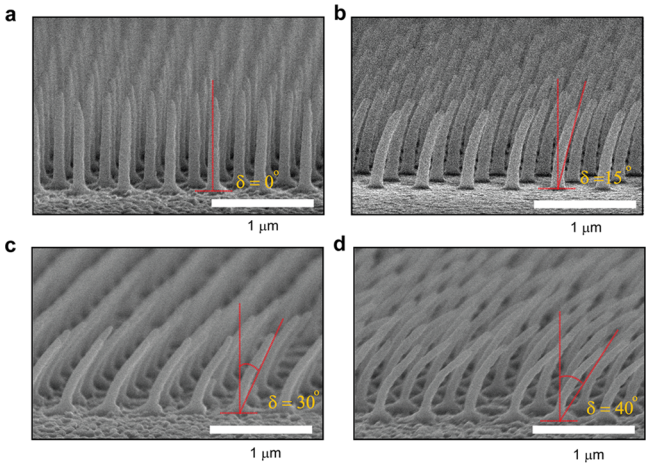


**Figure 4.** SEM images for geometry-controlled nanofiber arrays. (a) Vertical nanohair arrays. (b−d) Various tilted nanohairs by oblique broad ion beam irradiation: (b) $\delta$ = 15°, (c) 30°, and (d) 40°, respectively.

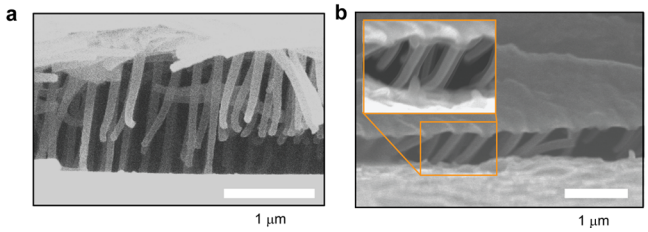


**Figure 5.** Cross-sectional SEM images of paired nanohairs for (a) vertical and (b) tilted nanohairs. Here, the geometry of nanohairs is the same: 50 nm radius, 1 $\mu$m height, and SR = 3 with hexagonal layout.

model is needed to quantitatively describe the measured adhesion forces for vertical and tilted hairs. Once the hairs are brought into contact by a uniformed preload, the hairs are paired by van der Waals forces ($F_{vdw}$) as shown in Figure 6a (step 1), in which $F_{vdw} = A(R)^{1/2} \cdot l/(16D_0^{2.5})$.[40] Here, $A$ is the Hamaker constant (∼2.09 × 10$^{-20}$ J for PU materials used in our experiment; see also Supporting Information), $R$ is the radius of nanohairs (50 nm), $D_0$ is the cutoff distance between hairs (0.4 nm), and $l$ is the overlapping length, which is approximately ∼70% of the total length of hairs as supported by the SEM images in Figure 5a,b. As illustrated in a series of steps 2−3, the interconnected nanohairs are displaced by an applied shear load and finally separated when $F_{vdw}$ is overwhelmed by the bending force, $F_{bending}$. Here, $F_{bending}$ may be viewed as an disjoining force to separate two surfaces, which can be expressed as $F_{bending} = 2EI\Delta\theta/(l_0 - l/2)^2$ assuming the condition of part-uniformly distributed load of beam deflection,[28] in which $I$ is the moment of inertia ($I = \pi \cdot R^4/4$), $E$ is the elastic modulus of the soft PUA material (∼19.8 MPa), and $l_o$ is total length of hair.

To derive a condition for the onset of separation, we introduce here an angle displacement from the initial interlocked position ($\Delta\theta$). Consequently, the maximum angular displacement ($\Delta\theta_m$) is given from the force balance between attractive $F_{vdw}$ and disjoining $F_{bending}$ such that $F_{bending} \sin\Delta\theta_m = \mu(F_{vdw} - F_{bending} \cos\Delta\theta_m)$ where $\mu$ is the frictional coefficient, ∼0.04.[28] After some algebraic manipulation, $\Delta\theta_m$


dx.doi.org/10.1021/am3009289 | ACS Appl. Mater. Interfaces 2012, 4, 4225−4230

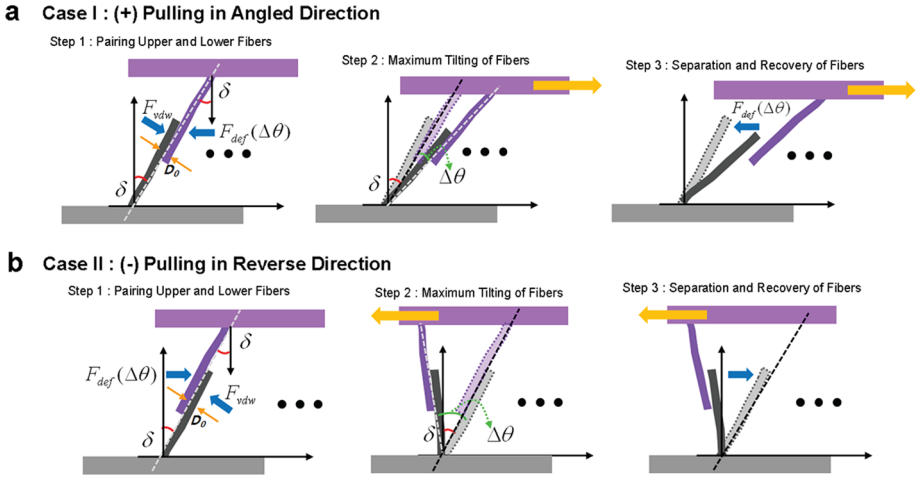


**Figure 6.** Illustrations for step-by-step events of bidirectional, asymmetric interlocking of single paired nanofibers in the (a) angled (+) and (b) reverse (−) directions. First, the upper and lower tilted nanofibers are paired (step 1), bended to the maximum angular displacement ($\Delta\theta_m$) before separation (step 2), and finally separated by external shear force (step 3).

can be simply expressed as a ratio between $F_{vdw}$ and $F_{bending}$, yielding

$$\Delta\theta_m \cong 0.6\mu\frac{F_{vdw}}{F_{bending}} \quad (1)$$

For the conditions used in our experiment, $\Delta\theta_m$ is approximated to 42° regardless of the pulling direction (see Supporting Information for detailed derivation).

Additionally, the shear adhesion force can be estimated from the $x$-component of the force vector, in which the separating angle is either given by $\Delta\theta_f = \delta + \Delta\theta_m$ (+ direction) or $\Delta\theta_f = \delta - \Delta\theta_m$ (− direction) considering the geometry of tilted nanohairs. Then one can have

$$F_{shear} = \rho F_{vdw}\cos(\delta \pm \Delta\theta_m), \ \{+: \text{angled}\} \text{ or } \{-: \text{reverse}\} \quad (2)$$

Here, $\rho$ is the pillar density per unit area ($\sim 18.5 \times 10^9/\text{cm}^2$) and $\delta$ is the initial tilting angle of nanohairs. Accordingly, the hysteresis ($H$) is given by

$$H = \frac{\rho F_{vdw}\cos(\delta - \Delta\theta_m)}{\rho F_{vdw}\cos(\delta + \Delta\theta_m)} \quad (3)$$

Figure 7a,b shows the measured adhesion forces and theoretical predictions when pulled in the (+) and (−) directions, respectively, as a function of $\delta$. In the angled direction, the measured force monotonically decreased from ~40 to ~20 N/cm$^2$ with the increase of $\delta$, which can be easily imagined intuitively as the hairs are initially angled in that direction. In the reverse direction, on the other hand, the force monotonically increased from ~40 to ~60 N/cm$^2$ with the increase of $\delta$, which also agrees with our intuition and the theoretical model in eq 2. Our theory indicates that the force would decrease with the increase of $\delta$ in the angled (+) direction (Figure 7a) while it would increase with the increase of $\delta$ in the reverse (−) direction (Figure 7b). Interestingly, the experimental data demonstate exellent agreement with these predictions except for slight deviations for higher initial tilting angles (>30°) in the (+) direction (Figure 7a). This is presumably due to the fact that the nanohairs are rather stooped, not straight, as a result of oblique broad beam

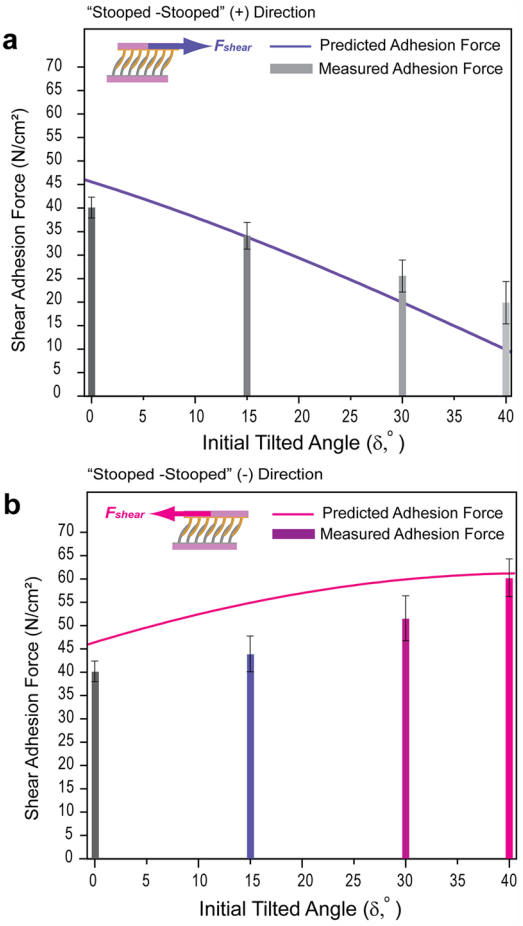


**Figure 7.** Comparisons of the measured shear adhesion forces with the theory using various tilting angles in the (a) angled (+) and (b) reverse (−) directions.

irradiation.[37,38] Also, the discrepancy may be associated with misalignment of upper and lower hairs and structural defects.

As with the microfiber arrays shown in Figure 3, the preload-dependent shear adhesion forces were measured in the range of 0.1 and 5 N/cm$^2$ (Figure 8a). Here, the maximum hysteresis is estimated to be ~7 for $\delta$ = 40°, which is substantially higher

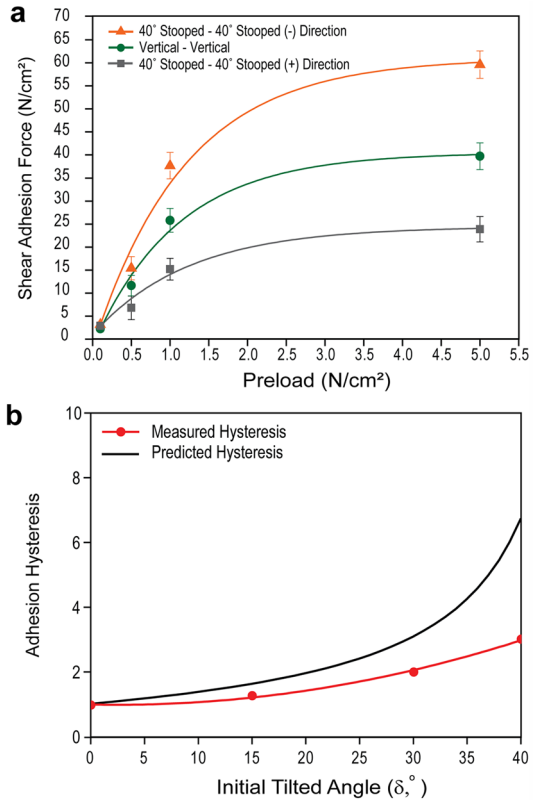


**Figure 8.** (a) Plots of preload dependency of shear adhesion force with 40° stooped−40° stooped and vertical nanofiber arrays. (b) Comparison of the measured adhesion hyteresis with the theory.

than the measured value of ∼3 (Figure 8b). This discrepancy seems also attributed to the same reasons mentioned above (stopped geometry, misalignment, structural defects, etc).

The durability of the current bidirectional interlocker was independently assessed, in which no notable reduction in the measured shear force was observed over 10 repeating cycles of attachment and detachment (Figure S4, Supporting Information). After that, the force was slowly deteriorated due to the continuous collapse and mating between neighboring hairs. It is noted in this regard that the mechanical strength of hairs could be substantially enhanced by coating a thin metal (e.g., Pt) layer of ∼5 nm at the expense of 10−20% reduction of the shear adhesion force.[37]

We also measured pulling forces with three different combinations of tilting angles in the reverse and forward directions: 40° stooped−40° stooped, vertical−vertical, 15° stooped−40° stooped (Supplementary Figure S5, Supporting Information). We found that the shear adhesion force between 15° stooped−40° stooped nanohairs was slighlty decreased as compared to 40° stooped−40° stooped hairs, probably due to the reduction of overlapping length between upper and lower hairs. To further demonstrate the utility of asymmetric adhesion, two pendulums (3 kg in − direction and 1 kg in + direction) were supported by 0.8 × 0.8 $cm^2$ patches with different pulling directions (Supplementary Figure S6, Supporting Information). Also, this asymmetric, bidirectional adhesion may be utilized as a simple, smart fastener to fix items with moderate weight when two different pulling forces are needed in a controllable fashion (Supplementary Figure S7, Supporting Information, with snapshots).

## SUMMARY

We have presented bidirectional, asymmetric interlocking between tilted micro- and nanohair arrays inspired from the actual wing locking device of beetles. The measured shear force turned out to be higher in the reverse direction than that in the angled direction, suggesting that the directionality of tilted microtrichia may play a critical role in preventing the elytra from shifting along the middle of insect body. A maximum shear locking force of ∼60 $N/cm^2$ was observed for the nanohair arrays of 50 nm radius and 1 $\mu$m height (SR = 3) with a hysteresis as high as ∼3. A simple theoretical model was developed to describe the measured asymmetric adhesion forces and the hysteresis, which were in good accordance with the experimental data.

## ASSOCIATED CONTENT

### Supporting Information

Calculation of Hamaker constants, detailed derivation of maximum angular displacement of hairs $\Delta\theta_m$, and supplemental figures (Figures S1−S5). This material is available free of charge via the Internet at http://pubs.acs.org.

## AUTHOR INFORMATION

### Corresponding Author

*Tel: +82-2-880-9103. Fax: +82-2-883-1597. E-mail: sky4u@snu.ac.kr.

### Author Contributions

§These authors contributed equally to this work.

### Notes

The authors declare no competing financial interest.

## ACKNOWLEDGMENTS

This work was supported by a National Research Foundation of Korea (NRF) grant (No. 20110017530), the WCU (World Class University) program (R31-2008-000-10083-0), the and Basic Science Research Program (2010-0027955). This work was supported in part by a Korea Research Foundation Grant (KRF-J03003) and the Global Frontier R&D Program on Center for Multiscale Energy System.

## REFERENCES

(1) Zheng, Y.; Bai, H.; Huang, Z.; Tian, X.; Nie, F. Q.; Zhao, Y.; Zhai, J.; Jiang, L. *Nature* **2010**, *463*, 640−643.
(2) Hou, Y. P.; Chen, Y.; Xue, Y.; Zheng, Y. M.; Jiang, L. *Langmuir* **2012**, *28*, 4737−4743.
(3) Parker, A. R.; Lawrence, C. R. *Nature* **2001**, *414*, 33−34.
(4) Zhai, L.; Berg, M. C.; Cebeci, F. C.; Kim, Y.; Milwid, J. M.; Rubner, M. F.; Cohen, R. E. *Nano Lett.* **2006**, *6*, 1213−1217.
(5) Neuhaus, S.; Spencer, N. D.; Padeste, C. *ACS Appl. Mater. Interfaces* **2012**, *4*, 123−130.
(6) Zheng, Y.; Gao, X.; Jiang, L. *Soft Matter* **2007**, *3*, 178−182.
(7) Malvadkar, N. A.; Hancock, M. J.; Sekeroglu, K.; Dressick, W. J.; Demirel, M. C. *Nat. Mater.* **2010**, *9*, 1023−1028.
(8) Duprat, C.; Protiere, S.; Beebe, A. Y.; Stone, H. A. *Nature* **2012**, *482*, 510−513.
(9) Reddy, S.; Arzt, E.; del Campo, A. *Adv. Mater.* **2007**, *19*, 3833−3837.
(10) Kwak, M. K.; Pang, C.; Jeong, H. E.; Kim, H. N.; Yoon, H.; Jung, H. S.; Suh, K. Y. *Adv. Funct. Mater.* **2011**, *21*, 3606−3616.
(11) Murphy, M. P.; Aksak, B.; Sitti, M. *Small* **2009**, *5*, 170−175.
(12) Bartlett, M. D.; Croll, A. B.; King, D. R.; Paret, B. M.; Irschick, D. J.; Crosby, A. J. *Adv. Mater.* **2012**, *24*, 994−994.
(13) Havener, M. B.; Sica, V.; Tang, T.; Jagota, A. *Langmuir* **2008**, *24*, 6182−6188.

(14) Gorb, E. V.; Gorb, S. N. *Beilstein J. Nanotechnol.* **2011**, *2*, 302−310.
(15) Bohn, H. F.; Federle, W. *Proc. Natl. Acad. Sci. U.S.A.* **2004**, *101*, 14138−14143.
(16) Greiner, C.; del Campo, A.; Arzt, E. *Langmuir* **2007**, *23*, 3495−3502.
(17) Kang, S. H.; Na, J. H.; Moon, S. N.; Lee, W. I.; Yoo, P. J.; Lee, S. D. *Langmuir* **2012**, *28*, 3576−3582.
(18) Chandra, D.; Yang, S.; Soshinsky, A. A.; Gambogi, R. J. *ACS Appl. Mater. Interfaces* **2009**, *1*, 1698−1704.
(19) Zhu, X. L.; Zhang, Y.; Chandra, D.; Cheng, S. C.; Kikkawa, J. M.; Yang, S. *Appl. Phys. Lett.* **2008**, *93*, 161911-1-3.
(20) Cui, Y. X.; Fung, K. H.; Xu, J.; Ma, H. J.; Jin, Y.; He, S. L.; Fang, N. X. *Nano Lett.* **2012**, *12*, 1443−1447.
(21) Dean, B.; Bhushan, B. *Philos. Trans. R. Soc., A: Math., Phys. Eng. Sci.* **2010**, *368*, 4775−4806.
(22) Hazel, J.; Stone, M.; Grace, M.; Tsukruk, V. *J. Biomech.* **1999**, *32*, 477−484.
(23) Xia, F.; Jiang, L. *Adv. Mater.* **2008**, *20*, 2842−2858.
(24) Kwak, M. K.; Jeong, H. E.; Kim, T. I.; Yoon, H.; Suh, K. Y. *Soft Matter* **2010**, *6*, 1849−1857.
(25) Hancock, M. J.; Sekeroglu, K.; Demirel, M. C. *Adv. Funct. Mater.* **2012**, *22*, 2223−2234.
(26) Gorb, S. N. *Proc. R. Soc. B: Biol. Sci.* **1999**, *266*, 525−535.
(27) Gorb, S. N. *Int. J. Insect Morphol.* **1998**, *27*, 205−225.
(28) Pang, C.; Kim, T. I.; Bae, W. G.; Kang, D.; Kim, S. M.; Suh, K. Y. *Adv. Mater.* **2012**, *24*, 475−479.
(29) Ko, H.; Lee, J.; Schubert, B. E.; Chueh, Y. L.; Leu, P. W.; Fearing, R. S.; Javey, A. *Nano Lett.* **2009**, *9*, 2054−2058.
(30) Shahsavan, H.; Zhao, B. X. *Langmuir* **2011**, *27*, 7732−7742.
(31) Vajpayee, S.; Khare, K.; Yang, S.; Hui, C. Y.; Jagota, A. *Adv. Funct. Mater.* **2011**, *21*, 547−555.
(32) Kapadia, R.; Ko, H.; Chueh, Y. L.; Ho, J. C.; Takahashi, T.; Zhang, Z.; Javey, A. *Appl. Phys. Lett.* **2009**, *94*, 263110-1-3.
(33) Kwak, M. K.; Jeong, H. E.; Suh, K. Y. *Adv. Mater.* **2011**, *23*, 3949−3953.
(34) Ko, H.; Zhang, Z. X.; Ho, J. C.; Takei, K.; Kapadia, R.; Chueh, Y. L.; Cao, W. Z.; Cruden, B. A.; Javey, A. *Small* **2010**, *6*, 22−26.
(35) Ko, H.; Zhang, Z.; Chueh, Y. L.; Saiz, E.; Javey, A. *Angew. Chem.* **2010**, *122*, 626−629.
(36) Pang, C.; Kang, D.; Kim, T. I.; Suh, K. Y. *Langmuir* **2012**, *28*, 2181−2186.
(37) Kim, T. I.; Jeong, H. E.; Suh, K. Y.; Lee, H. H. *Adv. Mater.* **2009**, *21*, 2279−2281.
(38) Rahmawan, Y.; Kim, T. I.; Kim, S. J.; Lee, K. R.; Moon, M. W.; Suh, K. Y. *Soft Matter* **2012**, *8*, 1673−1680.
(39) Choi, S. J.; Kim, H. N.; Bae, W. G.; Suh, K. Y. *J. Mater. Chem.* **2011**, *21*, 14325−14335.
(40) Israelachvili, J. N. *Intermolecular and Surface Forces: Revised*, Third ed.; Academic Press: 2011.